Arch. Metall. Mater. **64** (2019), 1, 387-392

DOI: 10.24425/amm.2019.126264

P. LACKI*#, K. ADAMUS*, J. WINOWIECKA*

THE NUMERICAL SIMULATION OF AVIATION STRUCTURE JOINED BY FSW

This work presents a numerical simulation of aviation structure joined by friction stir welding, FSW, process. The numerical simulation of aviation structure joined by FSW was created. The simulation uses thermomechanical coupled formulation. The model required creation of finite elements representing sheets, stiffeners and welds, definition of material models and boundary conditions. The thermal model took into account heat conduction and convection assigned to appropriate elements of the structure. Time functions were applied to the description of a heat source movement. The numerical model included the stage of welding and the stage of releasing clamps. The output of the simulation are residual stresses and deformations occurring in the panel. Parameters of the global model (the panel model) were selected based on the local model (the single joint model), the experimental verification of the local model using the single joint and the geometry of the panel joints.

Keywords: Aviation structure, friction stir welding, FSW, thermomechanical simulations, FEM

1. Introduction

The majority of numerical models describing FSW processes are based on computational fluid mechanics. Such models are useful in designing new tools [1], understanding the mechanism of defect formation [2] and developing techniques mitigating defect formation [3,4]. There are few thermomechanical models of FSW processes in literature. Most of them is focused on validation of calculated stresses [5-8]

Most of the thermomechanical simulations of conventional processes focus on components having thick cross-sections [1-3] and there are relatively few models of components having thin cross-section [4,5], i.e. components with thickness of 1 mm or lower. The major challenge is to extend the simulation capabilities from a model of a single weld to a model of a large structure containing multiple welds [4,6,7]. These structures are manufactured by joining sheets with stiffeners [8-11] or by forming technologies [12]. In the latter case they are called integrally stiffened panels (ISP). ISP structures can be joined using FSW [13] or Refill Friction Stir Spot Welding [14-18]. Compared to fusion welding technologies FSW offers better strength properties, fewer welding defects, reduction of welding distortions and reduction of residual stresses. Bulking loads of panels joined by FSW are lower than bulking loads of riveted panel. Both panel types have similar load carrying capabilities [19]. Thus, the reduction of heat input leads to the reduction of the welding distortions [20]. The longitudinal stiffeners contribute to reduction of buckling distortions [21]. The application of FSW to the structure comprising sheet and stiffeners produces the same pattern of deformations, however their magnitude is ignorantly lower [22]. Buckling tendencies in the welded panes are strongly dependent on the layout and the number of stiffeners [7]. The typical post-welding distortion in FSW processes is hyperbolic-parabolic deformation that occurs in single sheets as well as whole structures [22-24].

2. Numerical analysis of a single joint

The comparison of the joint macrostructure and the calculated temperature field in a cross-section was presented in Figures 1 and 2. The dark color in the macrostructure presents

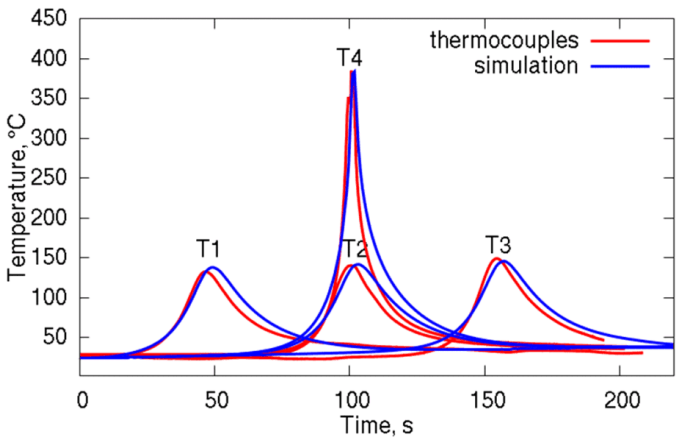

Fig. 1. The comparison of thermal cycles measured by thermocouples and calculated by the numerical model

* CZESTOCHOWA UNIVERSITY OF TECHNOLOGY, 69 DABROWSKIEGO STR., 42-201 CZESTOCHOWA, POLAND

Corresponding author: piotr@lacki.com.pl

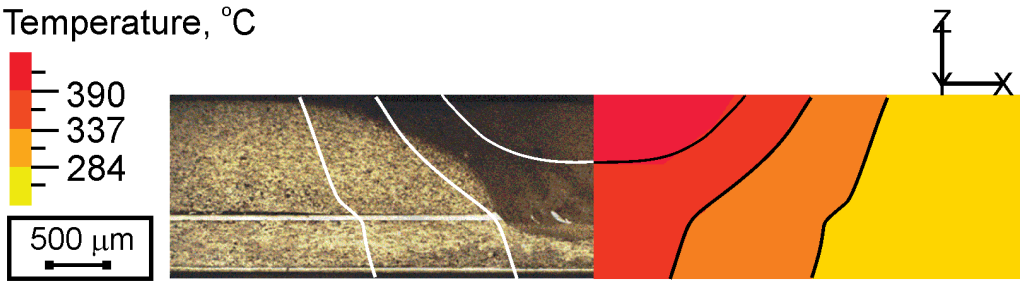

Fig. 2. The cross-section of FSW joint: left – macrostructure, right – simulation

the stir zone i.e. the volume of material where high temperature and high strain rates caused recrystallization of the material. The white horizonal lines are the anticorrosive aluminum coating of the D16 sheet (the bottom sheet).

The temperature field correspond to the time when highest temperature occurred in the section. The suggested heat source model, comprising the internal and the external parts, allows producing isotherms that match the shape of the stir zone. The 337°C isotherm approximately matches the outline of the stir zone. In the center of the joint there are significant temperature differences between the top and the bottom sheets due to heat generation by the FSW tool. Moving away from the weld, the differences diminish, however there is a horizontal offset in isotherms corresponding to the physical separation of the top and the bottom sheets.

The comparison of the actual joint and the calculated displacements in the direction perpendicular to the sheet top surface was presented in Figure 3. The longer edge of the top sheet bends in the downward direction. The corners of the actual joint were put on steel blocks and additional loads were put at the top of the corners to achieve the same level of the corners. Similarly, in the simulation the corner nodes were fixed at initial Z coordinates.

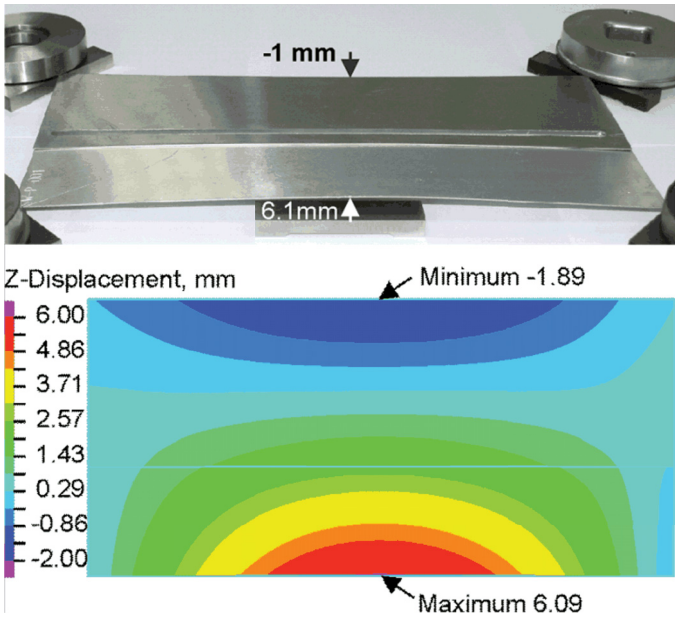

Fig. 3. The deformations of the FSW joint: the photo (top), the calculated displacement field

The actual displacement of the side edge in the bottom sheet is 6.1 mm and the calculated displacement is 6.09 mm. The actual displacement of the side edge in the top sheet is –1 mm and the calculated displacement is –1.89 mm. The discrepancy between the actual and the calculated maximal displacement of the side edge in the bottom sheet is below 1%. The discrepancy between the actual and the calculated maximal displacement of the side edge in the top sheet is below 89%.

3. Numerical analysis of aluminum panel

The numerical simulation of aviation structure joined by FSW was created. The simulation uses thermomechanical coupled formulation. The model required creation of finite elements representing sheets, stiffeners and welds, definition of material models and boundary conditions. The thermal model took into account heat conduction and convection assigned to appropriate elements of the structure. The numerical model included the stage of welding and the stage of releasing clamps. The output of the simulation are residual stresses and deformations occurring in the panel. Parameters of the global model (the panel model) were selected based on the local model (the single joint model), the experimental verification of the local model using the single joint and the geometry of the panel joints.

The three-dimensional model was based on the geometry of the panel. The panel has dimension 818.00 × 1623.93 mm. The panel comprises 3 parts: 1) the upper part consisting of a sheet having thickness of 0.8 mm and four stiffeners 2) the middle part with a window comprising a sheet having thickness of 1.5 mm and two stiffeners 3) the bottom part comprising a sheet having thickness 1.2 mm and 14 stiffeners. The stiffeners have the geometry of an L-profile (bracket) and a T-profile (tee).

The thermomechanical model was implemented in ADINA program which is based on finite element method. The thermal calculations were carried out in ADINA-T module, the mechanical calculations were carried out in ADINA model. The heat generated in the thermal module has impact of strains in the mechanical module. Boundary conditions were defined separately in the thermal and the mechanical modules.

The implementation of the model requires groups of finite element method for the sheets, the stiffeners, the welds and heat exchange between the panel and the surrounding environment (Fig. 4). The heat exchange was represented by convection

elements assigned to two types of surfaces. The first contact surfaces representing the heat exchange with air. The corresponding convection coefficient was set to 20 W/m^2·K. The second contact surfaces representing the heat exchange with clamping device. The corresponding convection coefficient was set to 100 W/m^2·K. These surfaces include surfaces of stiffeners and surfaces of sheets that have contact with clamping device.

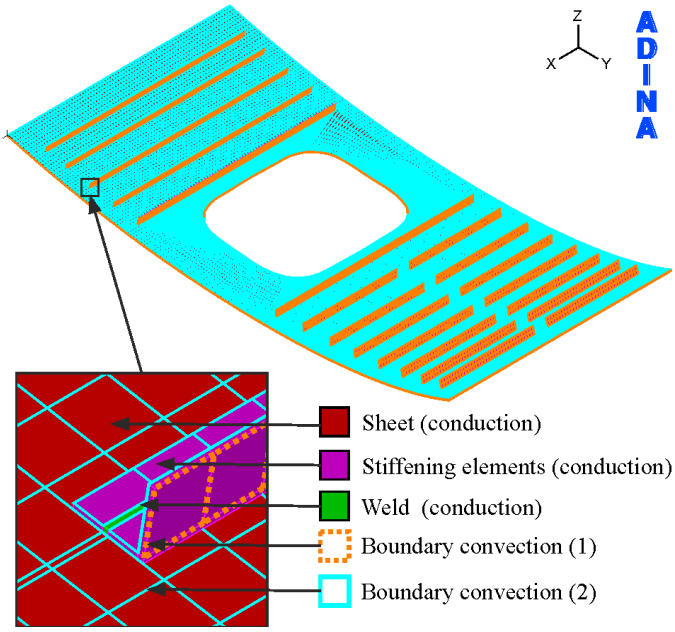

Fig. 4. The element groups in the thermomechanical model

The heat in three-dimensional thermal model is assigned to volumes representing the welds. The amount of heat generated by the heat source is chosen in such a way that the material reaches an appropriate temperature. It was assumed that that the power of the heat source is 200 W. The heat exchange was implemented at surfaces having contact with the surrounding air and the clamping device. The cooling of the panel was presented in Figure 5.

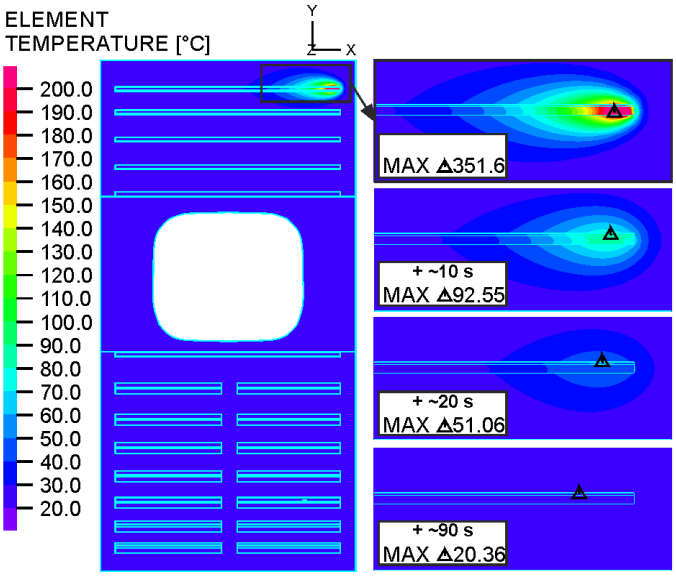

Fig. 5. The gradual cooling of the panel after 10, 20 and 90 seconds

The most intense period of cooling occurs during the first 10 seconds, subsequently the temperatures gradually drop to about 20°C. The maximal temperature achieved during welding is equal to 351.6°C. During 6 time steps, which correspond to the 10-second cooling period, as a result of convection and conduction, the maximal temperature drops by 74% to 92.55°C. After 20 seconds the maximum temperature drops to 51. 06°C, and after 90 s to 20.36°C.

In strategy (1), welding of each stiffener to a sheet begins at the end near the panel side and progresses toward the inner part of the panel. In the case of the bracket stiffeners, once the FSW tool reaches the middle of a stiffener, it is lifted and the welding process continues at the other end of the stiffener, again toward its middle. In the case of the tee stiffeners two welds are performed from the two side of each stiffener. The tee stiffeners are arrange into two columns. The welding progresses alternately between the left and the right column. The welding order and the direction of the welding tool movement is presented in Figure 6.

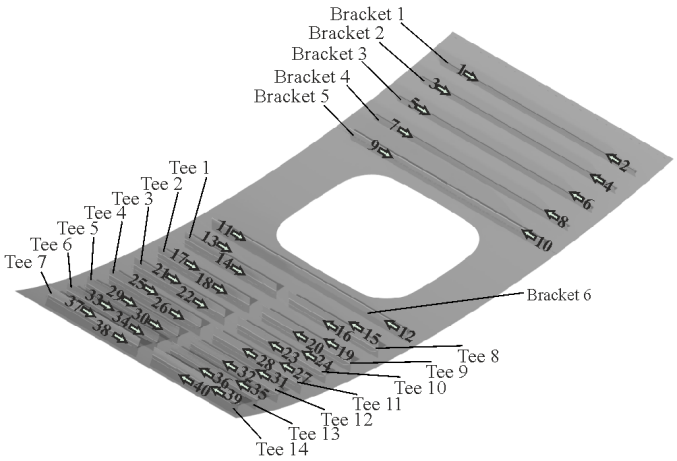

Fig. 6. The visualization of strategy (1)

The main assumption in strategy (2) is to delay consecutive welds so that the heat generated by a previous weld dissipate in the panel. The welding begins with the stiffener joining the middle part with the bottom part and the stiffener joining the middle part with the upper part. In the next stage welding process continues with the tee stiffeners in the bottom part and the bracket stiffeners in the upper part in such a sequence that there are at least two stiffeners between the next stiffener and the previous stiffener. The welding order and the direction of the welding tool movement is presented in Figure **7**.

In strategy (1) two delays between consecutive welds, having values of 10.32 and 89.44 s, were taken into account. In strategy (2) the delay between consecutive welds was equal to 10.32 s. Additionally two delay times (10.32 and 89.44 s) between the end of the welding and the beginning of the clamp release were taken into account.

Table 1 contains the summary of the numerical calculations for the two strategies. Displacement magnitude column contains the maximum displacement among all nodes at the end of simulation. This variable best summarizes the welding

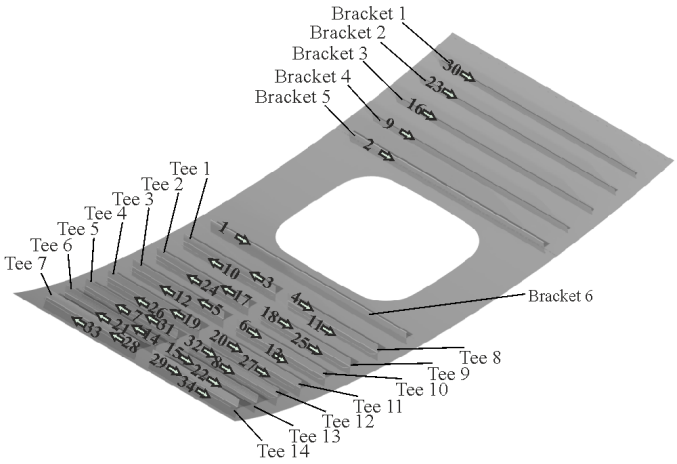

Fig. 7. The visualization of strategy (2)

deformations. For the delay time between consecutive welds of 10.32 s the displacement magnitude was 81.17 and 71.56 mm for strategies (1) and (2) respectively. By modifying the delay time between the welds and the delay time between the welding stage and the releasing clamps stage it is possible to decrease model deformations by 36 and 10 %.

TABLE 1

The summary of the simulation results

Strategy	Delay time, s	Cooling before unloading, s	Overall time, s	Effective stress, MPa	Displacement magnitude, mm
(1)	10.32	10.32	2659.9780	317.1	81.17
	89.44	89.44	5350.0519	317.5	51.90
(2)	10.32	10.32	2659.9780	309.4	71.56
	10.32	89.44	2727.9830	309.4	64.06

Figure 8 presents the residual stress distribution after the release of clamps for the two strategies, for the delay time between the welds equal to 10.32 s. In the case of the strategy 1 the maximal effective stress is equal to 317.1 MPa and in the case

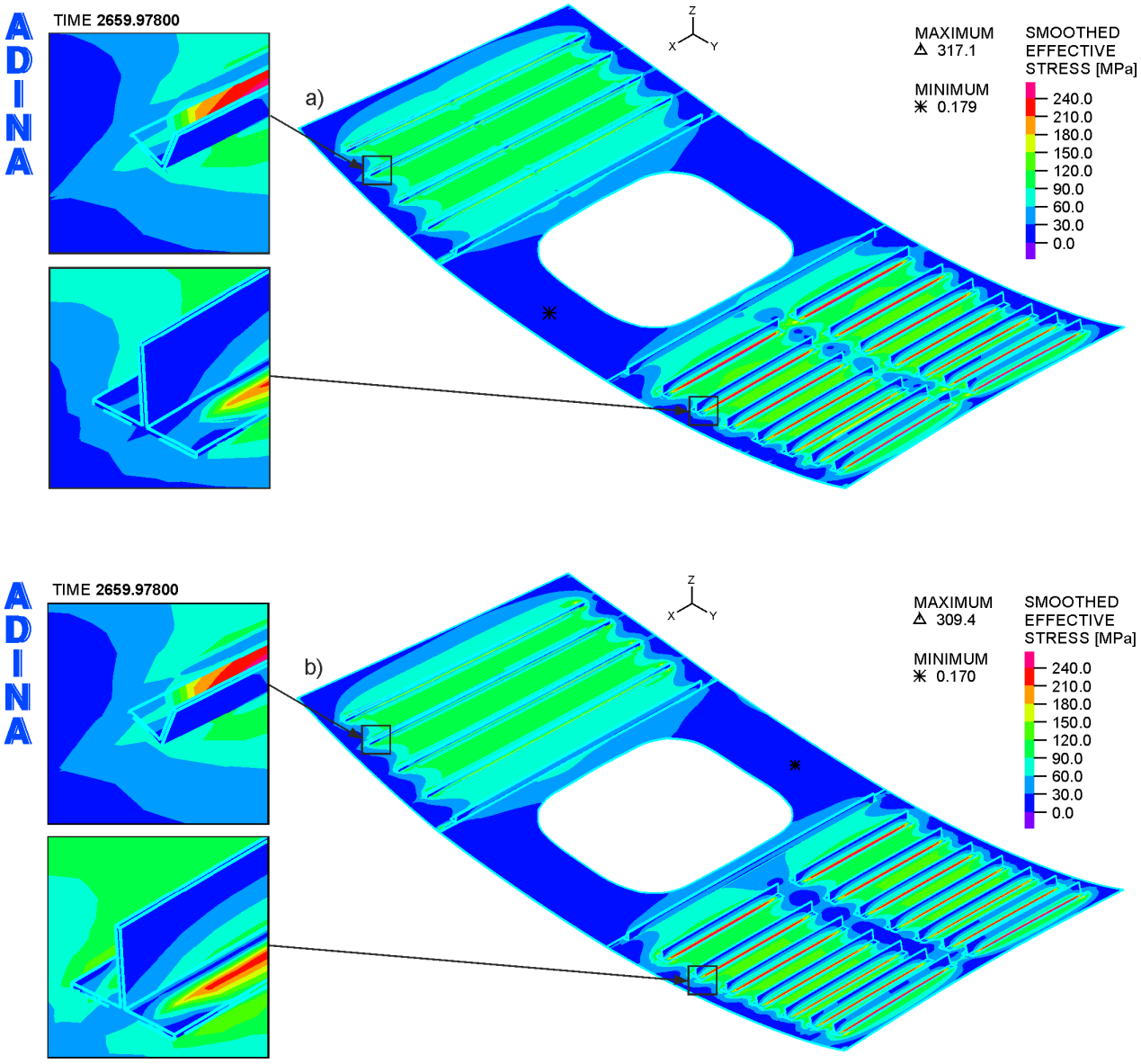

Fig. 8. The effective stress after the release of clamps (the delay time equal to 10.32 s) for strategy a) 1 i b) 2

of the strategy 2 it is equal to 309.4 MPa. The increase of the delay between the welds didn't contribute to significant change of the maximum stress.

Figure 9 presents the displacement magnitude distribution for the strategy 1 and the strategy 2 and for two delay times (10.32 s and 89.44 s). The maximum displacement magnitude occurs for the strategy 1 and the delay between the welds equal to 10.32 s. The lower displacement magnitude in the bottom part are the result of different joint geometry and different section thickness. Additionally the highest density of stiffeners occurs in the bottom part. For all of the analyzed cases the character of deformations is similar. The greatest deformations occurs in the corners of the panel.

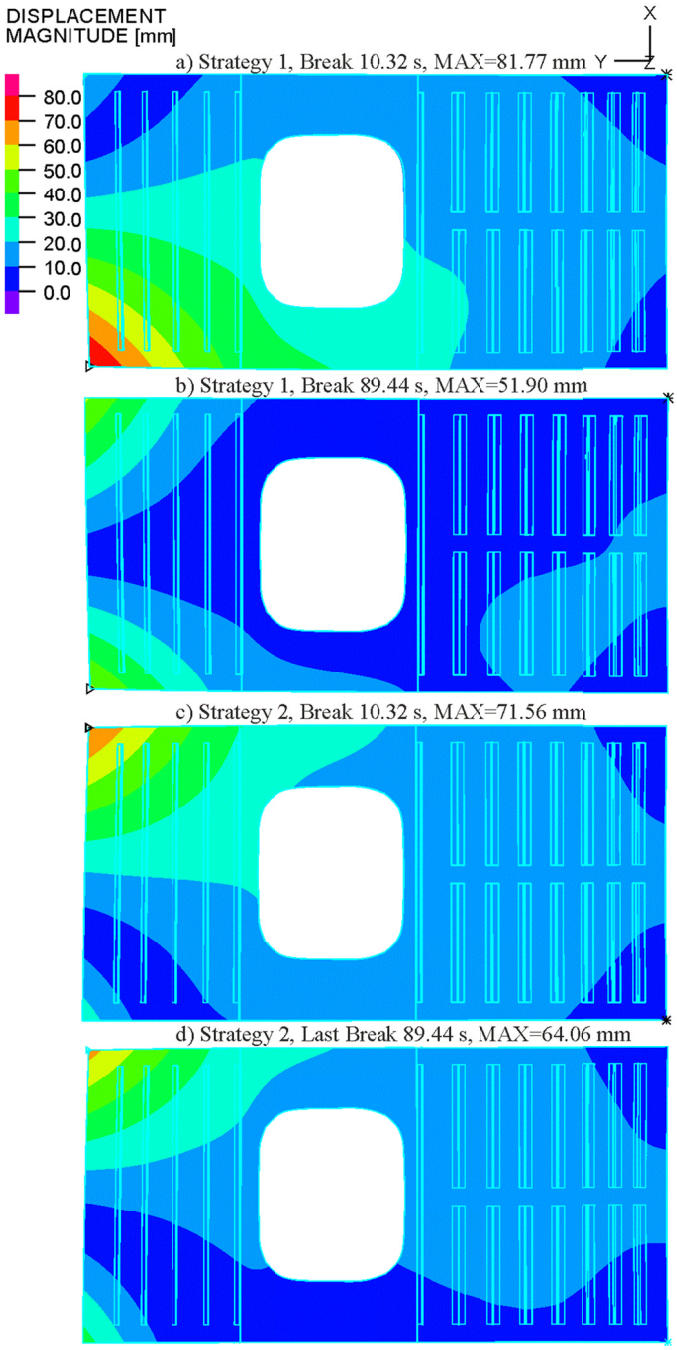

Fig. 9. The distribution of displacement magnitude for the strategies 1 and 2 and different delays between welds

4. Conclusions

1. It is possible to reduce deformations of the analyzed panel by applying the appropriate strategy of the FSW process. The lowest deformations were obtained for strategy 1 with the delay time between the welds extended to 90 s. The maximum displacement magnitude for this case was about 51.9 mm.
2. The best results were obtained by increasing the delay between the welds in order to dissipate the heat. For the strategy 2, the maximum displacement magnitude was about 72 mm. The extension of the delay caused the decrease of the displacement magnitude to 64 mm.
3. The increase of the delay between the welds that causes dissipation of the heat can decrease deformations by 36%. The increase of the delay between the welding stage and the release clamps stage to 90 s decreased the displacement magnitude by 10%.
4. The maximum values of residua stresses are almost identical for all analyzed cases and are in the range between 309.4 and 317.5 MPa. The largest stresses occur in welds.

Acknowledgments

Financial support of The National Centre for Research and Development, European Union, PZL Mielec / a Sikorsky Company, in the framework of European Regional Development Fund Project „Advanced techniques for the fabrication of airframe structures using innovative friction stir welding (FSW) technology", no. INNOLOT/I/4/NCBR/2013 is gratefully acknowledged.

REFERENCES

[1] K. Hemmesi, M. Farajian, M. Boin, Mater Design **126**, 339-350 (2017).
[2] D.F. Almeida, R.F. Martins, J.B. Cardoso, Procedia Struct. Integrity **5**, 633-639 (2017).
[3] M. Dal, R. Fabbro, Opt. Laser Technol. **78**, 2-14 (2016).
[4] H. Huang, S. Tsutsumi, J. Wang, L. Li, H. Murakawa, Finite Elem. Anal. Des. **135**, 1-10 (2017).
[5] A. Kouadri-Henni, C. Seang, B. Malard, V. Klosek, Materials & Design **123**, 89-102 (2017), DOI: 10.1016/j.matdes.2017.03.022.
[6] L. Xiu, J. Wu, Z. Liu, J. Ma, X. Fan, H. Ji, X. Xia, Y. Li, Fusion Eng. Des. **121**, 43-49 (2017), DOI: 10.1016/j.fusengdes.2017.03.175.
[7] N. Ma, J. Wang, Y. Okumoto, Int. J. Adv. Manuf. Technol. **41**, 4, 20 (2015), DOI: 10.1007/s00170-015-7810-y.
[8] S. Shroff, E. Acar, C. Kassapoglou, Thin Wall Struct. **119**, 235-246 (2017), DOI: 10.1016/j.tws.2017.06.006.
[9] M.C. Simmons, G.K. Schleyer, Thin Wall Struct. **44**, 5, 496-506 (2006), DOI: 10.1016/j.tws.2006.05.002.
[10] A. Singh, F. Yang, R. Sedaghati, Engineering Structures **159**, 99-109 (2018), DOI: 10.1016/j.engstruct.2017.12.040.

[11] B. Keshtegar, P. Hao, Y. Wang, Q. Hu, Appl. Soft Comput **66**, 196-207 (2018).

[12] J.F. Caseiro, R.A.F. Valente, A. Andrade-Campos, J.W. Yoon, International Journal of Mechanical Sciences **76**, 49-59 (2013), DOI: 10.1016/j.ijmecsci.2013.09.002.

[13] J.W. Yoon, G. H. Bray, R.A.F. Valente, T.E.R. Childs, Thin Wall Struct. **47**, 12, 1608-1622 (2009), DOI: 10.1016/j.tws.2009.05.003.

[14] A. Derlatka, P. Kasza, Advanced Materials Research **1020**, 151-157 (2014), DOI: 10.4028/www.scientific.net/AMR.1020.151.

[15] A. Derlatka, K. Kudła, K. Makles, Numerical analysis of RFSSW joints. in: E. Oñate, X. Oliver, A. Huerta (Eds.), 11th World Congress on Computational Mechanics (WCCM XI), Barcelona (2014).

[16] P. Lacki, A. Derlatka, Composite Structures **159**, 491-497 (2017), DOI: 10.1016/j.compstruct.2016.10.003.

[17] A. Derlatka, P. Kasza, Advanced Materials Research **1020**, 158-164 (2014), DOI: 10.4028/www.scientific.net/AMR.1020.158.

[18] P. Lacki, A. Derlatka, Composite Structures **202**, 201-209 (2018), DOI: 10.1016/j.compstruct.2018.01.050.

[19] Q. Shao, Y. He, T. Zhang, L. Wu, Chin. J. Mech. Eng. **27**, 4, 761-767 (2014), DOI: 10.3901/CJME.2014.0507.087.

[20] D. Deng, H. Murakawa, Computational Materials Scienc**e 43**, 4, 591-607 (2008), DOI: 10.1016/j.commatsci.2008.01.003.

[21] A. Murphy, W. McCune, D. Quinn, M. Price, Thin Wall Struct. **45**, 3, 339-351 (2007), DOI: 10.1016/j.tws.2007.02.007.

[22] D.-Y. Yan, A.-P. Wu, J. Silvanus, Q.-Y. Shi, Materials & Design **32**, 4, 2284-2291 (2011), DOI: 10.1016/j.matdes.2010.11.032.

[23] R.M.F. Paulo, P. Carlone, V. Paradiso, R.A.F. Valente, F. Teixeira-Dias, Thin-Walled Structures **120**, 297-306 (2017), DOI: 10.1016/j.tws.2017.09.009.

[24] Q.-Y. Shi, J. Silvanus, Y. Liu, D.-Y. Yan, H.-K. Li, Science and Technology of Welding and Joining **13**, 5, 472-478 (2013), DOI: 10.1179/174329308X341924.